Molecular modeling toward selective inhibitors of dihydrofolate reductase from the biological warfare agent Bacillus anthracis

ARTICLE *in* EUROPEAN JOURNAL OF MEDICINAL CHEMISTRY · JUNE 2014

Impact Factor: 3.45 · DOI: 10.1016/j.ejmech.2014.06.025 · Source: PubMed

European Journal of Medicinal Chemistry 91 (2015) 63–71

Contents lists available at ScienceDirect

European Journal of Medicinal Chemistry

journal homepage: http://www.elsevier.com/locate/ejmech

Original article

Molecular modeling toward selective inhibitors of dihydrofolate reductase from the biological warfare agent *Bacillus anthracis*

Juliana O.S. Giacoppo [a], Daiana T. Mancini [a], Ana P. Guimarães [b], Arlan S. Gonçalves [c], Elaine F.F. da Cunha [a], Tanos C.C. França [b], Teodorico C. Ramalho [a, *]

[a] *Laboratory of Computational Chemistry, Department of Chemistry, Federal University of Lavras (UFLA), Campus Universitário, PO Box 3037, 37200-000, Lavras, MG, Brazil*
[b] *Laboratory of Molecular Modeling Applied to the Chemical and Biological Defense, Military Institute of Engineering, Praça General Tiburcio 80, Urca, 22290-270, Rio de Janeiro, RJ, Brazil*
[c] *Federal Institute of Education Science and Technology of Espirito Santo (IFES), Avenida Ministro Salgado Filho S/N°, 29106-010, Vila Velha, ES, Brazil*

ARTICLE INFO

Article history:
Received 13 February 2014
Accepted 12 June 2014
Available online 18 June 2014

Keywords:
Bacillus anthracis
Inhibitors
Docking
Molecular dynamics
Biological warfare

ABSTRACT

In the present work, we applied docking and molecular dynamics techniques to study 11 compounds inside the enzymes dihydrofolate reductase (DHFR) from the biological warfare agent *Bacillus anthracis* (*Ba*DHFR) and *Homo sapiens sapiens* (*Hss*DHFR). Six of these compounds were selected for a study with the mutant *Ba*F96IDHFR. Our results corroborated with experimental data and allowed the proposition of a new molecule with potential activity and better selectivity for *Ba*DHFR.

1. Introduction

Bacillus anthracis, one of the most dangerous biological warfare agents, has already been employed as a weapon by both military and terrorist groups and is capable of causing high mortality rates, despite the therapy available today [1–3]. This microorganism is a gram-positive, aerobic, spore-forming bacterium that causes anthrax mainly in herbivorous animals but can also cause acute disease in humans [3–6]. *B. anthracis* exists in two morphologically distinct forms: the dormant spore (infectious form) and the metabolically active bacterium [7,8]. The spores are highly resistant and can withstand the intense stress generated by nature, persisting in the environment for long periods of time [9,10]. They can enter mammals hosts by three different ways (cutaneous, gastrointestinal and inhalation) each causing infection with specific symptoms [6]. The cutaneous infection occurs in about 95% of cases and the gastrointestinal and inhalation infections have higher mortality rates [11].

Current therapies against anthrax include penicillin, ciprofloxacin and tetracyclines [12]. However, prophylactic treatment requires these antibiotics being administered to patients before the onset of symptoms and the current vaccination strategies require the regular administration of reinforcements over a period of 18 months in order to maintain immunity [13,14]. This facts, together with the menace represented by the eventual use of *B. anthracis* as a biological agent, signal to the importance of the search for new targets to the drug design against anthrax.

The enzyme DHFR plays a key role in the folate pathway, responsible for the biosynthesis of deoxythymidine monophosphate, as well as of purine nucleotides and the amino acids histidine and methionine [15–17]. This enzyme catalyzes the reduction of dihydrofolate to tetrahydrofolate using NADPH as cofactor [18] and is essential for the survival of most living beings. DHFR is an important target largely studied in literature for several human diseases (protozoal, bacterial and fungal infections, psoriasis, autoimmune disease and neoplastic diseases) [16,19] and the DHFR from *B. anthracis* (*Ba*DHFR) has been seen as a suitable target to the drug design against anthrax [1,15,20,21]. Studies by Beirlein et al. [15,20] have shown that *B. anthracis* is resistant to the clinically used antifolate trimethoprim (TMP). In order to solve this problem Beirlein et al. [15] and Pelphrey et al. [21] synthesized and tested a new set of derivatives from propargyl as new effective antifolates against anthrax [15]. These compounds presented IC_{50} values between 0.80 and 30.50 μM, but low selectivity face to

* Corresponding author.
E-mail addresses: teodorico.ramalho@gmail.com, teo@dqi.ufla.br (T.C. Ramalho).

http://dx.doi.org/10.1016/j.ejmech.2014.06.025
0223-5234/

human DHFR (*Hss*DHFR). Beierlein et al. [20] also evaluated the resistance face TMP of mutants *Ba*F96IDHFR and *Ba*Y102FDHFR. Their results indicate that the mutant *Ba*Y102FDHFR is more sensitive to TMP while *Ba*F96IDHFR present almost the same sensibility observed for *Ba*DHFR.

In this work we used docking and molecular dynamics (MD) techniques to study the binding modes of the inhibitors proposed by Beirlein et al. [15] and Pelphrey et al. [21] inside the active sites of *Ba*DHFR, *Hss*DHFR and *Ba*F96IDHFR in order to investigate the molecular aspects essentials for the selectivity and propose new derivatives of these compounds potentially more selective to *Ba*DHFR.

Table 1
IC_{50} (μM) values of the DHFR compounds.

Compound	*Ba*DHFR	*Hss*DHFR	*Ba*F96IDHFR
1	0.89	1.28	8.90
2	0.94	0.06	0.52
3	1.30	1.30	1.96
4	1.70	3.20	–
5	2.30	1.46	–
6	3.70	0.40	0.50
7	4.80	1.46	–
8	9.20	0.13	–
9	14.50	5.71	1.91
10	29.10	1.22	2.76
11	30.30	1.38	–

2. Methodology

2.1. DHFR inhibitors studied

The structures of the compounds studied and their IC_{50} values with *Ba*DHFR, *Hss*DHFR and *Ba*F96IDHFR are shown in Fig. 1 and Table 1, respectively. Compounds **1**–**4** and **8** were synthesized by Beirlein et al. [15] while compounds **5**–**7** and **9**–**11** were synthesized by Pelphrey et al. [21]. The experimental results for mutant *Ba*F96IDHFR were obtained by Beirlein et al. [20].

2.2. Docking strategy

The 3D dimeric crystallographic structures of *Ba*DHFR (complexed with NADPH and 5-[3-(2,5-dimethoxyphenyl)prop-1-yn-1-yl]-6-ethylpyrimidine-2,4-diamine), *Hss*DHFR (complexed with NADPH and TMP) and *Ba*F96IDHFR (complexed with NADPH and TMP) were downloaded from the Protein Data Bank (PDB) server [22] under the codes 3E0B, 3W3A and 3JW3, respectively. Considering that the monomers are identical and independent of each other, we selected only the monomer A of each enzyme to perform our docking and MD studies [23]. Also, the co-crystallized water molecules were removed from both monomers using the software Molegro Virtual Docker (MVD®) [24].

The 3D structures of each compound in Fig. 1 were built using the program PC Spartan Pro® [25] and their partial atomic charges calculated by the RM1 semi-empirical method. The compounds were docked inside *Ba*DHFR, *Hss*DHFR and *Ba*F96IDHFR using MVD® [24] under a restriction sphere of radius 7 Å and considering the side chains of the residues within a radius of 11 Å as flexible. The binding modes of the ligands were determined as the lowest interaction energies of the enzyme–ligand complexes most associated to the bioactive conformations of 5-[3-(2,5-dimethoxyphenyl)prop-1-yn-1-yl]-6-ethylpyrimidine-2,4-diamine inside *Ba*DHFR and TMP inside *Hss*DHFR and *Ba*F96IDHFR.

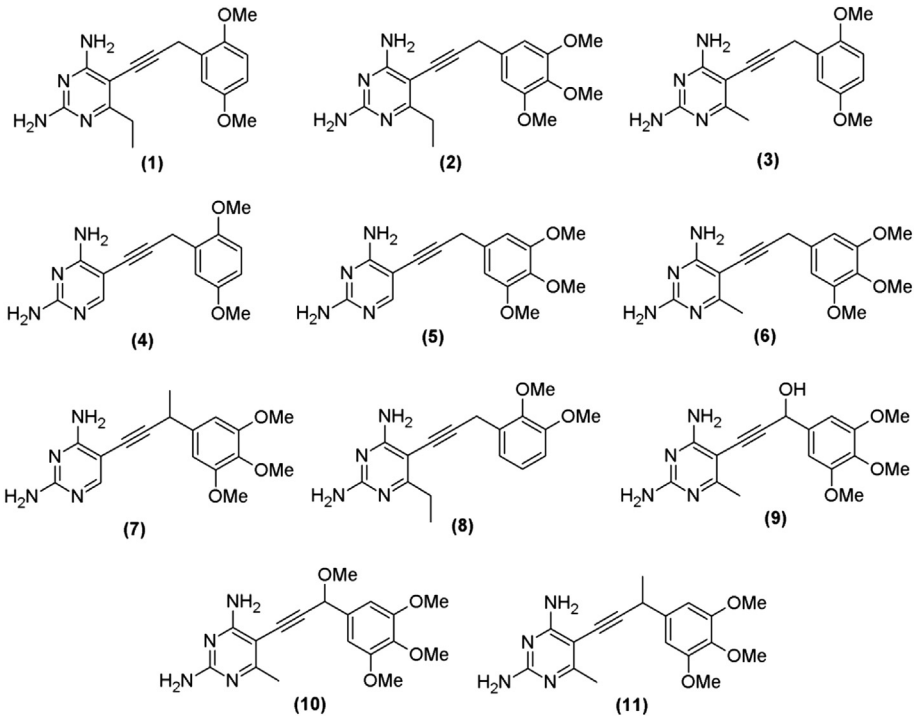

Fig. 1. Structures of the DHFR inhibitors studied. (1) 5-[3-(2,5-dimethoxyphenyl)prop-1-yn-1-yl]- 6-ethylpyrimidine-2,4-diamine; (2) 2,4-Diamino-5-[3-(3,4,5-trimethoxyphenyl) prop-1-ynyl]-6-ethylpyrimidine; (3) 2,4-Diamino-5-[3-(2,5-dimethoxyphenyl)prop-1-ynyl]-6-methylpyrimidine; (4) 2,4-Diamino-5-[3-(2,5-dimethoxyphenyl)prop-1-ynyl]pyrimidine; (5) 2,4-Diamino-5-(3-(3,4,5-trimethoxyphenyl)prop-1-ynyl)pyrimidine; (6) 2,4-Diamino-5-(3-(3,4,5-trimethoxyphenyl)prop-1-ynyl)-6-methylpyrimidine; (7) 2,4-Diamino-5-(3-(3,4,5 trimethoxyphenyl)but-1-ynyl)pyrimidine; (8) 2,4-Diamino-5-[3-(2,3-dimethoxyphenyl)prop-1-ynyl]-6-ethylpyrimidine; (9) 3-(2,4-Diamino-6-methylpyrimidin-5-yl)-1-(3,4,5-trimethoxyphenyl) prop-2-yn-1-ol; (10) 2,4-Diamino-5-(3-methoxy-3-(3,4,5-trimethoxyphenyl)prop-1-ynyl)-6 methylpyrimidine; (11) 2,4-Diamino-5-(3-(3,4,5-trimethoxyphenyl)but-1-ynyl)-6-methylpyrimidine.

Due to the stochastic nature of the docking algorithm, about 15 runs were performed for each compound and 30 poses (conformation and orientation of the ligand) were returned to the analysis of the overlap with the compounds present in the 3D structures of the enzymes studied and the ligand–enzyme interactions. The best pose of each compound was selected for the subsequent MD simulation steps.

The docking protocol described above was validated, before application, by re-docking studies.

2.3. Molecular dynamics studies

Before performing the MD simulations it was necessary to parameterize the ligands so they could be recognized by the forcefield OPLS/AA [26] from the program GROMACS 4.5 [27]. To obtain the parameters and topologies for the referred compounds, we used the AnteChamber PYthon Parcer InterfacE (ACPYPE) [28]. It is a tool based on PyThon programming language to use ANTECHAMBER (currently bundled in AmberTools version 1.4) [29] to generate parameters and topologies for chemical compounds and to interface with other Python applications like CCPN tools [30] or ARIA2 [31]. ACPYPE is currently able to generate output files for the following MM softwares: CNS/XPLOR [32,33] GROMACS [27], CHARMM [34] and AMBER [35]. The software MKTOP [36] was used to generate the parameters that were not given by ACPYPE [28]. OPLS/AA [26] forcefield parameters for the ligands were used and the atomic partial charges were calculated by semi-empirical quantum chemistry SQM [37] via ANTECHAMBER, according to AM1-BCC parameters (parameterized to reproduce HF/6-31G RESP charges). SQM was modified to include six decimals of precision instead of the default 3. The enzyme/ligands/NADPH complexes were simulated using the GROMACS 4.5 package [27] in cubic boxes of approximately 364,885 nm^3 containing around 10,600 water molecules. These systems were minimized using the OPLS/AA [26] forcefield. The minimization algorithms used were steepest descent with position restrained (PR) of the ligands and convergence criterion of 100.00 kcal mol^{-1} $Å^{-1}$, followed by steepest descent without PR, conjugate gradients and, finally, quasi Newton Raphson until an energy of 1.00 kcal mol^{-1} $Å^{-1}$. The minimized complexes were, then, submitted to MD simulations in two steps. Initially, we performed 500 ps of MD, at 310 K and physiologic pH, with PR, at NVT state, for the entire system, except the water molecules, in order to ensure a balance of the solvent molecules around the residues of the protein. Subsequently, there were performed 10 ns of MD simulations, at NPT state, 310 K and physiologic pH, without any restriction, using 2 fs of integration time and a cut-off of 10 Å for long-distance interactions. A total of 500 conformations were obtained during each simulation. In this step, the lists of pairs (pairlists) were updated every 500 steps and all Arg and Lys residues were assigned with positive charges and the residues Glu and Asp were assigned with negative charges, in order to reproduce their protonation states under physiologic conditions.

To analyze the structures generated after the optimization and MD steps, we used the visual molecular dynamics (VMD) [38] and Swiss-Pdb Viewer [39] programs. Plots of variation of total energy, distance, variation of random mean square deviation (RMSD) and H-bonds formed during the MD simulation were generated with the Origin program [40]. Qualitative spatial RMSD pictures were generated in the MolMol [41] and the figures of the frames of MD simulations were generated in the PyMOL program [42].

3. Results and discussion

3.1. Docking study of BaDHFR and HssDHFR

The re-docking results for the best-docked structures of 5-[3-(2,5-dimethoxyphenyl)prop-1-yn-1-yl]-6-ethylpyrimidine-2,4-diamine and TMP inside *Ba*DHFR and *Hss*DHFR presented RMSD values for the superpositions (see Fig. S1 in Supporting information) of the non-hydrogen atoms of 0.814 Å for *Ba*DHFR and 1.020 Å for *Hss*DHFR, respectively. Considering that literature reports a RMSD value lower than 2.00 Å as acceptable [43–45] these results validate the docking protocol used.

The volumes of the active site cavities of *Ba*DHFR and *Hss*DHFR, calculated by MVD® [24], were of 295.4 $Å^3$ and 473.1 $Å^3$, respectively. The ligand–enzyme interaction energies were calculated inside these cavities in order to provide a better understanding of the relationships between the binding modes of the ligands and the molecular factors responsible for activity.

Tables S1 and S2 list the docking energy values obtained in our work and the pIC_{50} values reported by Beirlein et al. [15] and Pelphrey et al. [21] for each compound inside *Ba*DHFR and *Hss*DHFR. As can be seen, the higher the pIC_{50} the lower the intermolecular energy. This is in full agreement with the experimental results reported by those authors as illustrated by the good correlations ($R^2 = 0.925$ and 0.904, respectively) in the plots of Fig. 2 and Fig. S2 (Supporting information).

Tables 2 and 3 list the residues present in interactions, the energies and pIC_{50} values of the most selective compounds towards *Ba*DHFR and *Hss*DHFR, according to the results shown in Table S1 and S2 (Supporting information). These Tables present only the results of four compounds (**1**, **11**, **4** and **3**) selected using the criteria of selectivity which is evaluated by the experimental IC_{50} values (Table 1).

As can be seen in Table 2, compound **1** presents the lowest energy of interaction (−144.05 kcal mol^{-1}) which could mean potentially better interactions with the active site of *Ba*DHFR and, therefore, higher inhibition. This compound interacts by H-bonds with three amino acid residues of the active site of *Ba*DHFR: Met06, Glu28 and Thr115. For *Hss*DHFR, we noticed that the interaction energy value of compound **1** increases to −138.48 kcal mol^{-1}, revealing H-bond interactions with Ile7, Glu30, Tyr121, Thr136 and NADPH. Aiming selectivity this energy difference becomes a favorable point for further studies of these interactions and the structure of this compound, subsequently, enabling a proposal of a new possible inhibitor.

Compound **11** presents a worse interaction energy value than the others (−106.27 kcal mol^{-1}), showing less interactions with

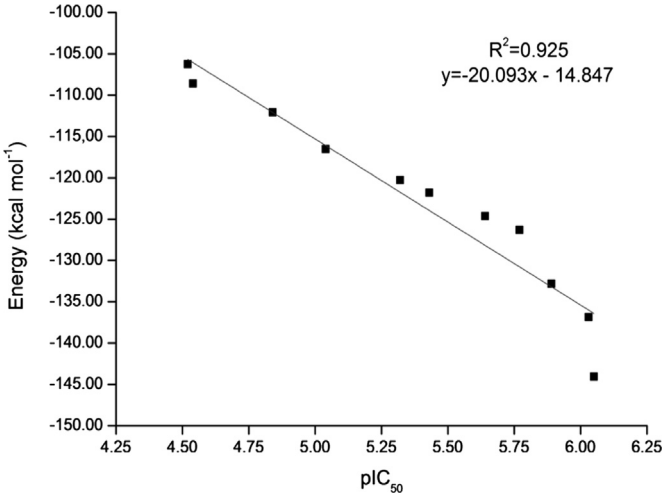

Fig. 2. Experimental *versus* theoretical results. Correlation between the intermolecular interaction energies (kcal mol^{-1}) and pIC_{50} (μM) for compounds 1–11 inside *Ba*DHFR [15].

Table 2
Docking results for compounds **1**, **3**, **4** and **11** inside *Ba*DHFR and their pIC_{50} values.

Compound	Residue	Distance (Å)	Bond strength (kcal mol^{-1})	ΔE[a] (kcal mol^{-1})	H-bond energy (kcal mol^{-1})	pIC_{50}
1[b]	Met6	2.65	−1.34	−144.05	−8.64	6.05
	Thr115	3.22	−1.88			
	Glu28	2.97	−1.98			
	Glu28	2.70	−2.50			
3	Glu28	3.23	−1.84	−132.82	−8.77	5.89
	Met6	2.58	−2.32			
	Phe96	3.13	−2.34			
	Tyr102	3.15	−2.26			
	Cofactor	3.12	−2.39			
	Cofactor	2.23	−1.85			
4	Glu28	3.23	−1.87	−126.30	−8.09	5.77
	Phe96	3.13	−2.36			
	Tyr102	3.33	−1.36			
	Met6	2.72	−2.50			
	Cofactor	3.32	−1.40			
	Cofactor	2.93	−2.50			
11	Glu28	3.43	−0.86	−106.27	−3.36	4.52
	Thr115	2.97	−2.50			
	Cofactor	3.59	−0.07			

[a] ΔE = Intermolecular energy.
[b] Re-docking.

the active site of *Ba*DHFR, thus a low inhibition potential. This result is in agreement with the experimental values. This compound presents three H-bond interactions, one with NADPH, and the others with residues Glu28 and Thr115. With *Hss*DHFR compound **11** presents a decrease in the interaction energy as expected (Table 3). Residues Ile7, Ala9, Tyr121, Thr136 and NADPH are responsible for its stability and higher affinity for the active site of *Hss*DHFR.

Similarly, compound **4** shows a variation in the interaction energy, from −126.30 kcal mol^{-1} (*Ba*DHFR) to −124.76 kcal mol^{-1} (*Hss*DHFR). Molecular interactions were observed with NADPH and residues Ile7, Tyr121, Thr136 inside *Hss*DHFR. This compound was also examined more carefully as a lead for new compounds.

Compound **3** presents interaction energies of −132.82 and −138.40 kcal mol^{-1} with *Ba*DHFR and *Hss*DHFR respectively. This small difference in terms of interaction energy is in very good agreement with experimental data.

3.2. Molecular dynamics simulations of BaDHFR and HssDHFR

After docking studies, all the **11** compounds were submitted to MD simulations in order to observe their dynamic behavior inside *Ba*DHFR and *Hss*DHFR and compare to the docking results, obtaining additional information to support the proposition of new potential inhibitors of *Ba*DHFR.

The temporal RMSD calculations were performed on all the atoms of each complex studied to 500 frames at every 10 ps, during the 10 ns of simulation. Considering that the complexes could fluctuate in the box, each frame was adjusted by the least squares method to its previous one for the calculation of the standard deviation. As observed for the systems *Ba*DHFR/Compound **1** and *Hss*DHFR/Compound **1** the temporal RMSD (Figs. 3 and S3 in Supporting information) tends to stabilize in the first ps of simulation. This behavior was common to all simulations, with deviations never exceeding 3.3 Å and 2.2 Å for enzyme and ligand, respectively. These results suggest that the ligands accommodated

Table 3
Docking results for compounds **1**, **3**, **4** and **11** inside *Hss*DHFR and their pIC_{50} values.

Compound	Residue	Distance (Å)	Bond strength (kcal mol^{-1})	ΔE[a] (kcal mol^{-1})	H-bond energy (kcal mol^{-1})	pIC_{50}
1	Ile7	2.99	−2.50	−138.48	−7.06	5.89
	Glu30	3.46	−0.82			
	Tyr121	3.24	−1.82			
	Thr136	3.22	−1.92			
	Cofactor	2.62	−2.50			
3	Ile7	2.75	−2.50	−138.40	−8.17	5.89
	Ala9	3.49	−0.01			
	Glu30	3.44	−0.78			
	Tyr121	3.12	−2.41			
	Thr136	3.10	−2.47			
	Cofactor	3.02	−2.50			
4	Ile7	2.75	−2.50	−124.76	−5.78	5.49
	Tyr121	3.13	−2.33			
	Thr136	3.41	−0.95			
	Cofactor	3.01	−2.50			
11	Ile7	3.33	−1.33	−138.38	−3.87	5.86
	Ala9	3.30	−0.03			
	Tyr121	3.50	−0.50			
	Thr136	3.20	−2.01			
	Cofactor	2.75	−2.50			

[a] ΔE = Intermolecular energy.

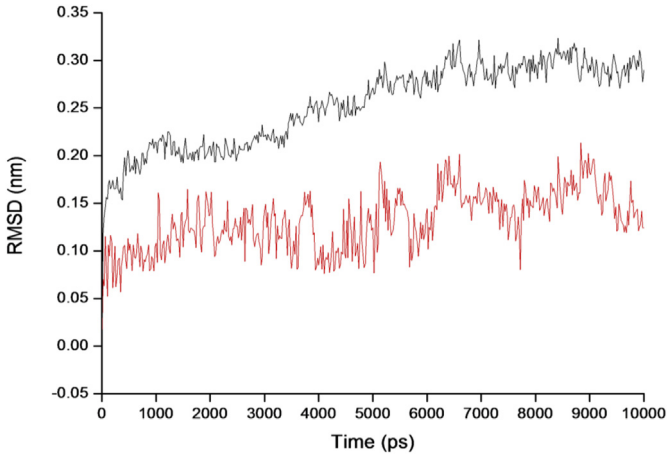

Fig. 3. Temporal RMSD of the system *Ba*DHFR/Compound **1** during MD simulation. The enzyme curve is shown in black and the compound curve is shown in red. (For interpretation of the references to color in this figure legend, the reader is referred to the web version of this article.)

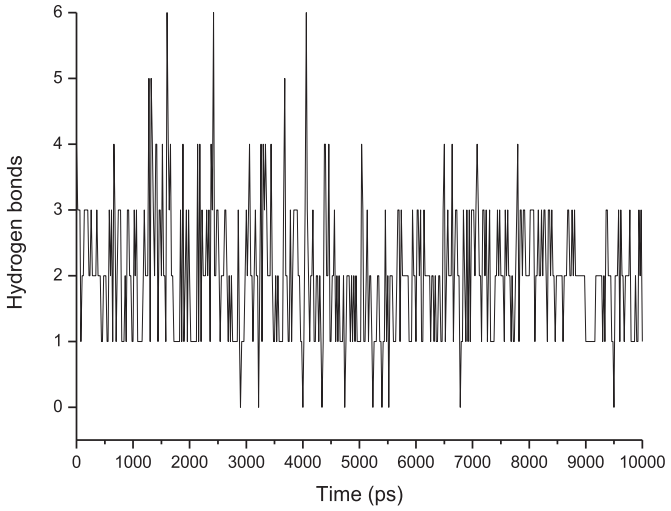

Fig. 5. Number of H-bonds. Interactions between compound **1** and *Ba*DHFR during the MD simulation.

well inside the active sites during the MD simulation, showing stabilization of the systems.

The sequence of frames from the MD simulation of Compound **1** inside *Ba*DHFR, presented in Fig. 4A, shows that this compound remains stabilized inside the active site, where it interacts with residues Met06, Glu28 and Thr115. This result confirms the stability of the MD simulation and the strong interaction with the enzyme, suggested by the total energy (data not shown) and RMSD plots. Similar results were observed in the docking studies, suggesting the greater stability of this molecule inside *Ba*DHFR. This stability can be an important factor to explain its better inhibitory power observed experimentally [15].

According to the docking studies, Compound **1** is able to form H-bond interactions with tree residues of the active site of *Ba*DHFR. Similar result was obtained in the MD simulation, showing the formation of up to 6 H-bonds with the permanence of 1–3 (Fig. 5).

The succession of frames for compound **1** inside the active site of *Hss*DHFR (Fig. 4B) shows that this compound stayed among residues Ile7, Glu30, Tyr121, Thr136 and the cofactor during the simulation time. According to the docking study, this compound carried out H-bonds with five residues inside *Hss*DHFR. During the MD simulation, we have observed the formation of 8 interactions prevailing up 2–4 H-bonds, as seen in Fig. S4 (Supporting information).

3.3. Docking study of BaDHFR and BaF96IDHFR

Previous studies from Beierlein et al. [20] showed that residues Phe96 and Tyr102 can play an important role in the natural resistance to TMP in *Ba*DHFR and a series of antifolates. Thus, those authors studied the two mutant enzymes *Ba*F96IDHFR and *Ba*Y102FDHFR. Their enzyme inhibition assays showed that the TMP, and several of the antifolates have significantly higher affinity

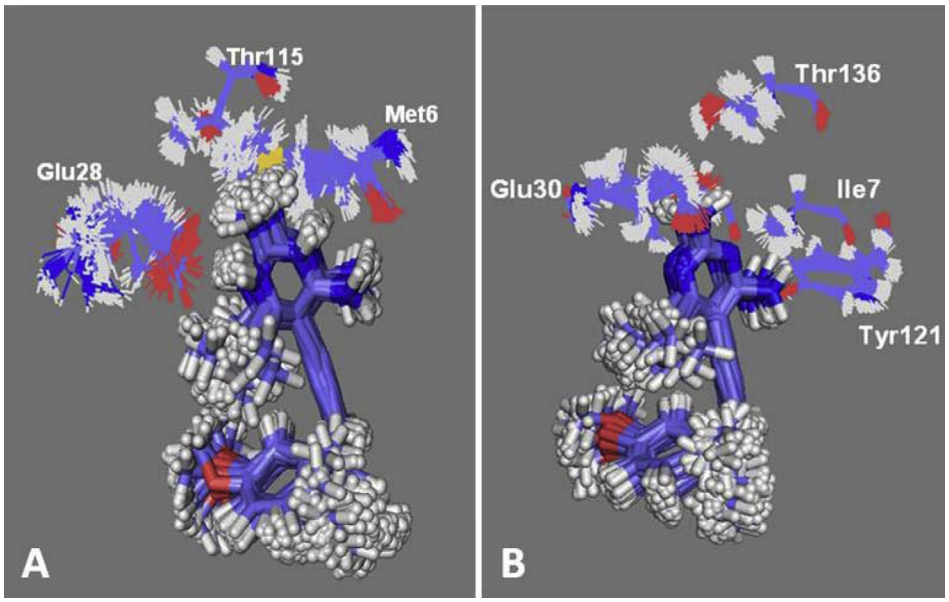

Fig. 4. Dynamic frames. **A**) Compound **1** inside the active site of *Ba*DHFR during the MD simulation. **B**) Compound **1** inside the active site of *Hss*DHFR during the MD simulation. The cofactor was omitted for better visualization.

for mutant *Ba*Y102FDHFR and approximately equal affinity for *Ba*F96IDHFR, suggesting that the residue Tyr102 is important in defining more powerful compounds. In order to get important features of the enzyme and propose compounds that would be effective also for *Ba*F96IDHFR, we performed additional docking and molecular dynamics studies on this mutant.

Six compounds were selected, which present the experimental results for both enzymes. Table 4 lists the docking energy values obtained in our work and the pIC_{50} values reported by Beirlein et al. [15,20] and Pelphrey et al. [21] for these compounds inside *Ba*DHFR and *Ba*F96IDHFR. As can be seen, the higher the pIC_{50} the lower the intermolecular energy. This is in full agreement with the experimental results reported by Beirlein et al. [15,20] and Pelphrey et al. [21] as illustrated by the good correlations ($R^2 = 0.945$ and 0.784 respectively) in the plots of Figs. S5 and S6 in Supporting information.

Differently from the previous results shown for *Ba*DHFR where compound **1** showed to be the best and more selective compound (Tables S1 and S2 in Supporting information) it now presented the worse energy value −105.57 kcal mol^{-1} and less efficient interactions (Table 5). Compound **6** showed to be more stable inside the active site of the mutant with an energy value of −131.44 kcal mol^{-1}. Through Table 5, we observe that this result is favored by interactions with residues Met6, Leu21, Glu28, Ile96, Tyr102, Thr115 and an interaction with NADPH. Fig. S7 shows the interactions of compounds **1** and **6** inside the active site of the mutant enzyme.

It is important to note that the 6 compounds studied presented interactions with residue Ile96. From Table 2, where we reported the residues of the active site of *Ba*DHFR, it can be observed that not all compounds interact with Phe96. So this mutation indeed influences the interaction with the site, but looking at the energy values we notice that compounds showing good results with *Ba*DHFR no longer show such promising results with *Ba*F96IDHFR.

3.4. Molecular dynamics simulations of BaDHFR and BaF96IDHFR

Fig. 6 shows the succession of frames of MD for compounds **1** and **6** inside *Ba*F96IDHFR. As can be seen in both simulations the compounds remained in the active site. This fact confirms the good interaction with the enzyme, corroborating the docking results.

3.5. Proposal for prototype inhibitor

Considering selectivity we observed that compounds **1** and **4** presented promising results, both experimentally and theoretically, suggesting to be the most selective for *Ba*DHFR. Thus, the structures of these compounds were analyzed more carefully as leads to the drug design of more selective inhibitors for *Ba*DHFR.

It is worth mentioning that all studied compounds are structurally very similar, so any change in the position of atoms or replacement of more or less bulky groups in their structure, influences the conformation in the active site of the enzyme, and, consequently, the activity.

Based on this and analyzing the structures of compounds **1**, **3** and **4** (Fig. 1) it is noticeable that the only difference among them is at the position of group R_1 (See Fig. 1). While in compound **1** R_1 is an ethyl group, in **3** it is a methyl and in **4** it is replaced by hydrogen. We noticed that bulkier substituents lead to lower IC_{50} values in both enzymes, fact that does not favor selectivity. So we also analyzed the structures of compounds **5**, **6**, **7** and **8** (Fig. 1), which differ only in the position of group R_2, and observed that by replacing the OMe group (compound **7**) by OH (compound **6**) the IC_{50} value for *Ba*DHFR decreased while increased for *Hss*DHFR. Thus, we selected the OH group as one of groups to be replaced. Another group chosen was NH_2, which has been tested with the intention of evaluating the electronic effect.

Based on these analysis we proposed modifications on the structures of these compounds at positions R_1 and R_2 as shown in Fig. 7. Table 6 presents the modifications performed and the interaction energy values obtained by docking studies after changes made in the structures of compounds **1** and **4** that originated prototypes **12** and **13**.

The intermolecular interaction energy between the prototype **13** and *Ba*DHFR decreased while with *Hss*DHFR no significant differences were observed, so it can be inferred that there was a modification to increase the stability of the compound in the active site of the *Ba*DHFR, which favors the issue of selectivity. Furthermore, for prototype **13** the difference between the values of

Table 4
Docking results and pIC_{50} ($pIC_{50} = -\log IC_{50}$ (μM)) values for compounds **1**, **2**, **3**, **6**, **9** and **10** inside *Ba*DHFR and *Ba*F96IDHFR.

Compound	*Ba*DHFR		*Ba*F96IDHFR	
	pIC_{50}	Intermolecular energy (kcal mol^{-1})	pIC_{50}	Intermolecular energy (kcal mol^{-1})
1	6.05	−144.05	5.05	−105.57
2	6.03	−136.85	6.28	−128.73
3	5.89	−132.82	5.71	−127.06
6	5.43	−121.80	6.30	−131.44
9	4.84	−112.09	5.72	−125.42
10	4.54	−108.60	5.56	−114.60

Table 5
Docking results for compounds **1**, **2**, **3**, **6**, **9** and **10** inside *Ba*F96IDHFR and their pIC_{50} values.

Comp	Residue	Distance (Å)	Bond strength (kcal mol^{-1})	ΔE^* (kcal mol^{-1})	H-bond energy (kcal mol^{-1})	pIC_{50}
1	Met6	2.53	−1.93	−105.57	−9.02	5.05
	Glu28	3.02	−2.50			
	Ile96	3.19	−2.01			
	Tyr102	3.20	−2.00			
	Thr115	3.49	−0.57			
	Cofactor	3.20	−1.99			
2	Met6	2.84	−2.02	−128.73	−7.94	6.28
	Glu28	3.34	−1.32			
	Ile96	3.20	−2.02			
	Thr115	3.18	−2.11			
3	Met6	2.52	−1.85	−127.06	−9.70	5.71
	Ala8	3.31	−0.03			
	Glu28	2.68	−2.50			
	Asn47	3.39	−0.32			
	Ile96	3.14	−2.28			
	Tyr102	3.20	−1.98			
	Cofactor	3.27	−1.62			
	Cofactor	3.20	−1.98			
6	Met6	2.44	−1.21	−131.44	−10.95	6.30
	Leu21	3.30	−1.26			
	Glu28	2.82	−2.50			
	Ile96	3.17	−2.16			
	Tyr102	3.12	−2.42			
	Thr115	3.32	−1.41			
	Cofactor	3.21	−1.96			
9	Met6	2.59	−2.38	−125.42	−10.93	5.72
	Val7	2.97	−0.68			
	Glu28	2.78	−2.50			
	Asn47	2.80	−2.50			
	Ile96	3.53	−0.37			
	Thr115	3.05	−2.50			
10	Met6	3.44	−0.78	−114.60	−8.27	5.56
	Glu28	3.05	−2.50			
	Asp47	2.60	−1.84			
	Ile96	2.99	−2.50			

*ΔE = Intermolecularenergy.

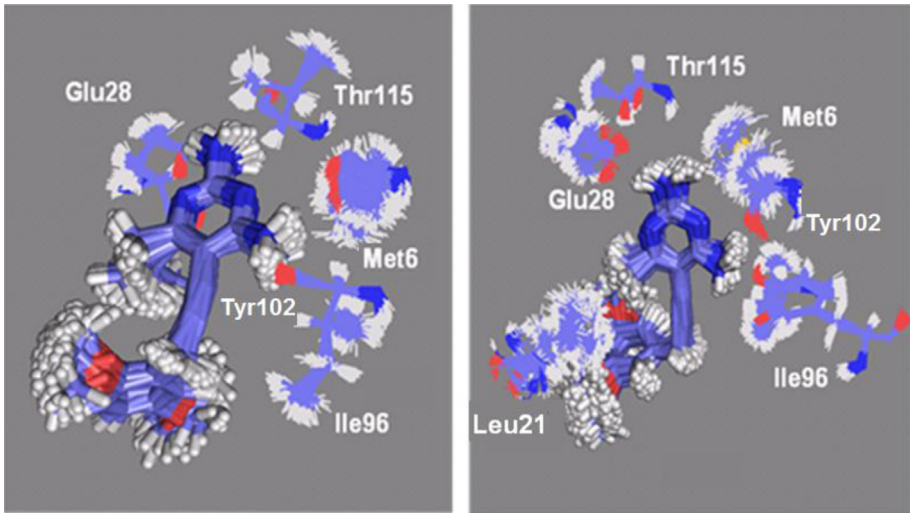

Fig. 6. Dynamic frames. Compounds 1 (left) and 6 (right) inside *Ba*F96IDHFR during the MD simulation. The cofactor was omitted for better visualization.

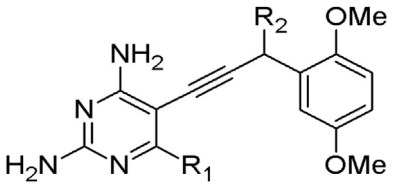

Fig. 7. Proposal structure. Structure to be modified at positions R_1 and R_2.

interaction energy inside *Ba*DHFR and *Hss*DHFR increased from 1.54 to 17.30 kcal mol^{-1}.

Similarly, there was a significant difference in energy values between prototype **12** and compound **1**. Ongoing from −144.05 kcal mol^{-1} to −156.28 kcal mol^{-1} in the interaction energy in the active site of *Ba*DHFR and −138.48 kcal mol^{-1} to −136.53 kcal mol^{-1} in the interaction energy with residues of *Hss*DHFR. Thus, resulting in a difference of 19.75 kcal mol^{-1} between the interaction energy values inside *Ba*DHFR and *Hss*DHFR active sites. These changes did not implied in large variation in the stability of the compounds in the active site of the human enzyme, but in relation to *Ba*DHFR a significant increase in stability was observed. Based on these results we selected prototype **12** for more detailed study.

Docking studies revealed that prototype **12** carries seven interactions which favor its stability. In addition to the interactions observed for compound **1**, this prototype also presents interactions with NADPH, Asn47 and Tyr102. Inside *Hss*DHFR, we observed the same interactions observed for compound **1** except for the interaction with the residue Glu30. The insertion of the −OH group resulted in no new interaction as evidenced in the small variation in interaction energies presented in Table 6.

Fig. S8 (Supporting information) shows the succession of frames of MD for prototype **12** inside *Ba*DHFR and *Hss*DHFR. As can be seen in both simulations this prototype remained in the active site. This fact confirms the good interaction with the enzyme, corroborating the docking results. The RMSD results for both enzymes were the same observed for compound **1**, confirming the stability of this prototype inside *Ba*DHFR and *Hss*DHFR during the simulated time.

It is noteworthy that other groups, such as −OMe, $-CH_3$, $-NH_2$, −OH, $-CH_2OH$ and $-CH_2CH_3$, were also tested in both positions, but did not show favorable results. It was observed that for both compounds **1** and **4** with the more bulky substituents there was an improvement in the energy of interaction between the compound and the active site of *Hss*DHFR, which is not favorable for our work. This effect can be explained by the larger cavity of *Hss*DHFR that accommodates better the inhibitor.

Docking studies with the enzyme *Ba*F96IDHFR showed that after modification of compound **1** in **12** by replacing the −OH group, the energy value has decreased from −105.57 kcal mol^{-1} to −116.58 kcal mol^{-1}, resulting in a significant difference (11.01 kcal mol^{-1}). This makes our prototype presents the best affinity to the active site which can represent better inhibitory capacity for this enzyme. The interactions observed between **12** and *Ba*F96IDHFR are reported in Fig. 8.

Fig. 9 shows the succession of frames of MD for prototype **12** inside *BaF96I*DHFR. As can be seen in the simulation this prototype remained in the active site. This fact confirms the good interaction with the enzyme, corroborating the docking results. Thus prototype **12** presents good results for *Ba*DHFR as well as good selectivity with

Table 6
Modifications performed and estimated values of intermolecular energy (kcal mol^{-1}) used for evaluation of the best binding modes.

Compound	Modification	*Ba*DHFR	*Hss*DHFR	*Ba*F96IDHFR	(I.E. *Hss*)–(I.E. *Ba*)[a] (kcal mol^{-1})
		Int. energy (kcal mol^{-1})	Int. energy (kcal mol^{-1})	Int. energy (kcal mol^{-1})	
1	–	−144.05	−138.48	−105.57	5.57
12[b]	R_2 = OH	−156.28	−136.53	−116.58	19.75
4	–	−126.30	−124.76	–	1.54
13[b]	$R_1 = CH_3$ e R_2 = OH	−140.73	−123.43	–	17.30

[a] I.E. *Hss*: Intermolecular energy for *Hss*DHFR; I.E. *Ba*: Intermolecular energy for *Ba*DHFR.
[b] New compounds proposed.

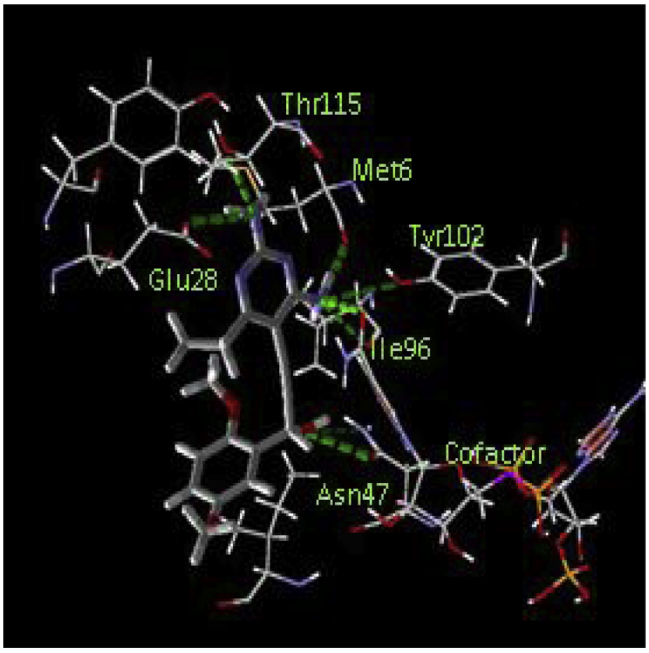

Fig. 8. Hydrogen interactions. Molecular interactions between prototype **12** and *Ba*F96IDHFR.

respect to *Hss*DHFR. Furthermore, this prototype has better theoretical results than compound **1** for the mutant *Ba*F96IDHFR.

4. Conclusions

The energies obtained in the docking studies indicated a good correlation between the theoretical and experimental data, corroborating the results of Beierlein et al. [15] that pointed compound **1** as the best *Ba*DHFR inhibitor.

The results obtained by MD simulations confirmed the docking studies, showing that these compounds remain well stabilized and anchored inside the active sites of both enzymes during the simulated time in all the studied systems.

Compound **1** was chosen as the most promising lead for new prototypes of inhibitors for *Ba*DHFR, based on their experimental results and theoretical good overall result. Through modifications on its structure we also proposed prototype **12** that, in turn, showed promising theoretical results. So, we propose this prototype for further experimental investigation.

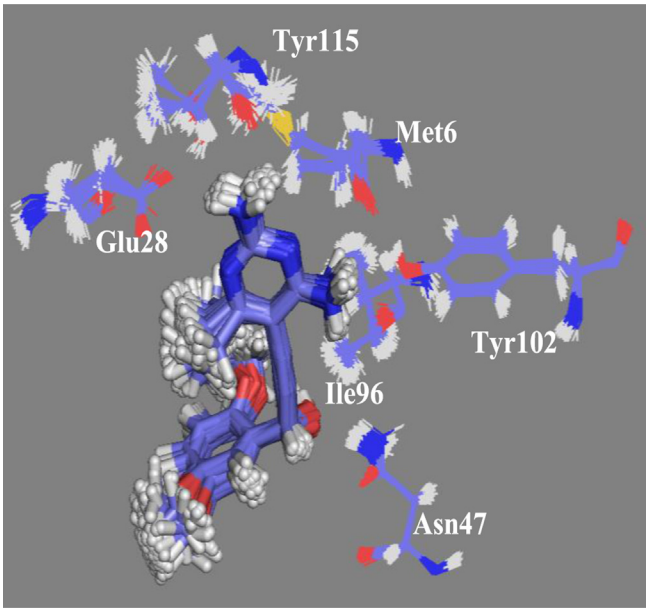

Fig. 9. Dynamic frames. Prototype **12** inside *Ba*F96IDHFR. The cofactor was omitted for better visualization.

Author contributions

Conceived and designed the experiments: TCR, TCCF. Performed the experiments: JOSG, DTM, APG. Analyzed the data: JOSG, ASG, TCCF. Contributed reagents/materials/analysis tools: ASG, EFFC. Wrote the paper: JOSG, TCR, TCCF.

Acknowledgments

The authors wish to thank the Brazilian financial agencies Conselho Nacional de Desenvolvimento Científico e Tecnológico (CNPq), grant no 304557/2012-9 and 474757/2012-9, Fundação de Amparo ao Ensino e Pesquisa do Estado do Rio de Janeiro (FAPERJ), grandt no. E-26/102.993/2012, Fundação de Amparo ao Ensino e Pesquisa de Minas Gerais (FAPEMIG), grant no. PPM-00499-13 and PPM-00434-13 and Coordenação de Aperfeiçoamento de Pessoal de Nível Superior/Ministério da Defesa (CAPES/MD) (Edital PRODEFESA 2008), grant no. PD 1782/2008 for financial support, and the Military Institute of Engineering (IME) and Federal Univesity of Lavras (UFLA) for providing the physical infrastructure and working space.

Appendix A. Supplementary data

Supplementary data related to this article can be found at http://dx.doi.org/10.1016/j.ejmech.2014.06.025.

References

[1] A.P. Guimarães, A.A. Oliveira, E.F.F. da Cunha, T.C. Ramalho, T.C.C. França, Analysis of *Bacillus anthracis* nucleoside hydrolase via *in silico* docking with inhibitors and molecular dynamics simulation, J. Mol. Model. 17 (2011) 2939–2951.
[2] D.L. Goldman, C. Arturo, Anthrax-associated shock, Front. Biosci. 13 (2008) 4009–4014.
[3] L.M. Irenge, J.L. Gala, Rapid detection methods for *Bacillus anthracis* in environmental samples: a review, Appl. Microbiol. Biotechnol. 93 (2012) 1411–1422.
[4] Y. Kurosaki, T. Sakuma, A. Fukuma, Y. Fujinami, K. Kawamoto, N. Kamo, S.I. Makino, J. Yasuda, A simple and sensitive method for detection of *Bacillus anthracis* by loop-mediated isothermal amplification, J. Appl. Microbiol. 107 (2009) 1947–1956.
[5] R.P. Verma, C. Hansch, Combating the threat of anthrax: a quantitative structure-activity relationship approach, Mol. Pharm. 5 (2008) 745–759.
[6] P.E.J. Carlson, S.D. Dixon, B.K. Janes, K.A. Carr, T.D. Nusca, E.C. Anderson, S.E. Keene, D.H. Sherman, P.C. Hanna, Genetic analysis of petrobactin transport in *Bacillus anthracis*, Mol. Microbiol. 75 (2010) 900–909.
[7] K.A. Carr, S.R. Lybarger, E.C. Anderson, B.K. Janes, P.C. Hanna, The role of *Bacillus anthracis* germinant receptors in germination and virulence, Mol. Microbiol. 75 (2010a) 365–375.
[8] K.A. Carr, B.K. Janes, P.C. Hanna, Role of the gerP operon in germination and outgrowth of *Bacillus anthracis* spores, PLoS One 5 (2010b) e9128–9134.
[9] G. Chen, A. Driks, K. Tawfiq, M. Mallozzi, S. Patil, *Bacillus anthracis* and *Bacillus subtilis* spore surface properties and transport, Colloids Surf. B. 76 (2010) 512–518.
[10] Y. Li, P. Catta, K.A. Stewart, M. Dufner, P. Setlow, B. Hao, Structure-based functional studies of the effects of amino acid substitutions in GerBC, the C subunit of the *Bacillus subtilis* GerB spore germinant receptor, J. Bacteriol. 193 (2011) 4143–4152.
[11] M. Meric, A. Willke, B. Muezzinoglu, A. Karadenizli, T. Hosten, A case of pneumonia caused by *Bacillus anthracis* secondary to gastrointestinal anthrax, Int. J. Infect. Dis. 13 (2009) e456–463.
[12] C.R. Bourne, R.A. Bunce, P.C. Bourne, K.D. Berlin, E.W. Barrow, W.W. Barrow, Crystal structure of *Bacillus anthracis* dihydrofolate reductase with the

dihydrophthalazine-based trimethoprim derivative RAB1 provides a structural explanation of potency and selectivity, Antimicrob. Agents Chemother. 53 (2009) 3065–3073.
[13] B.C. Bennett, H. Xu, R.F. Simmerman, R.E. Lee, C.G. Dealwis, Crystal structure of the anthrax drug target, *Bacillus anthracis* dihydrofolate reductase, J. Med. Chem. 50 (2007) 4374–4381.
[14] B.C. Bennett, Q. Wan, M.F. Ahmad, P. Langan, C.G. Dealwis, X-ray structure of the ternary MTX-NADPH complex of the anthrax dihydrofolate reductase: a pharmacophore for dual-site inhibitor design, J. Struct. Biol. 166 (2009) 162–171.
[15] J. Beierlein, K. Frey, D. Bolstad, P. Pelphrey, T. Joska, A. Smith, N. Priestley, D. Wright, A. Anderson, Synthetic and crystallographic studies of a new inhibitor series targeting *Bacillus anthracis* dihydrofolate reductase, J. Med. Chem. 51 (2008) 7532–7540.
[16] X.M. Li, M. Hilgers, M. Cunningham, Z.Y. Chen, M. Trzoss, J.H. Zhang, L. Kohnen, T. Lam, C. Creighton, G.C. Kedar, K. Nelson, B. Kwan, M. Stidham, V. Brown-Driver, K.J. Shaw, J. Finn, Structure-based design of new DHFR-based antibacterial agents: 7-aryl-2,4-diaminoquinazolines, Bioorg. Med. Chem. Lett. 21 (2011) 5171–5176.
[17] B. Nammalwar, R.A. Bunce, K.D. Berlin, C.R. Bourne, P.C. Bourne, E.W. Barrow, W.W. Barrow, Synthesis and biological activity of substituted 2,4-diaminopyrimidines that inhibit *Bacillus anthracis*, Eur. J. Med. Chem. 54 (2012) 387–396.
[18] J.M. Beierlein, L. Deshmukh, K.M. Frey, O. Vinogradova, A.C. Anderson, The solution structure of *Bacillus anthracis* dihydrofolate reductase yields insight into the analysis of structure-activity relationships for novel inhibitors, Biochemistry 48 (2009) 4100–4108.
[19] M. Sharma, P.M. Chauhan, Dihydrofolate reductase as a therapeutic target for infectious diseases: opportunities and challenges, Future Med. Chem. 4 (2012) 1335–1365.
[20] J.M. Beierlein, N.G. Karri, A.C. Anderson, Targeted mutations of *Bacillus anthracis* dihydrofolate reductase condense complex structure-activity relationships, J. Med. Chem. 53 (2010) 7327–7336.
[21] P. Pelphrey, V. Popov, T. Joska, J. Beierlein, E. Bolstad, Y. Fillingham, D. Wright, A. Anderson, Highly efficient ligands for DHFR from *Cryptosporidium hominis* and *Toxoplasma gondii* inspired by structural analysis, J. Med. Chem. 50 (2007) 940–950.
[22] H.M. Berman, J. Westbrook, Z. Feng, G. Gilliland, T.N. Bhat, H. Weissig, I.N. Shindyalov, P.E. Bourne, The protein data bank, Nucleic Acids Res. 28 (2000) 235–242.
[23] R.H. O'neil, R.H. Lilien, B.R. Donald, R.M. Stroud, A.C. Anderson, Phylogenetic classification of protozoa based on the structure of the linker domain in the bifunctional enzyme, dihydrofolate reductase-thymidylate synthase, J. Chem. Biol. 278 (2003) 52980–52987.
[24] R. Thomsen, M.H. Christensen, MolDock: a new technique for high accuracy molecular docking, J. Med. Chem. 49 (2006) 3315–3332.
[25] W.J. Hehre, B.J. Deppmeier, P.E. Klunzinger, PC SPARTAN Pro, Wavefunction, Inc., Irvine, CA, 1999.
[26] W.L. Jorgensen, J. Tirado-Rives, The OPLS force field for proteins. Energy minimizations for crystals of cyclic peptides and crambin, J. Am. Chem. Soc. 110 (1988) 1657–1666.
[27] B. Hess, C. Kutzner, D. Van der Spoel, E. Lindahl, GROMACS 4: algorithms for highly efficient, load-balanced, and scalable molecular simulation, J. Chem. Theo. Comput. 4 (2008) 435–447.
[28] A.W. Sousa da Silva, W.F. Vranken, ACPYPE – AnteChamber PYthon Parser interface, BMC Res. Notes 5 (2012) 367–374.
[29] J. Wang, W. Wang, P.A. Kollman, D.A. Case, Automatic atom type and bond type perception in molecular mechanical calculations, J. Mol. Graph. Mod. 25 (2006) 247–260.
[30] W.F. Vranken, W. Boucher, T.J. Stevens, R.H. Fogh, A. Pajon, M. Llinas, E.L. Ulrich, J.L. Markley, J. Ionides, E.D. Laue, The CCPN data model for NMR spectroscopy: development of a software pipeline, Proteins Struct. Funct. Bioinform. 59 (2005) 687–696.
[31] W. Rieping, M. Habeck, B. Bardiaux, A. Bernard, T.E. Malliavin, M. Nilges, ARIA2: automated NOE assignment and data integration in NMR structure calculation, Bioinformatics 23 (2007) 381–382.
[32] A.T. Brunger, Version 1.2 of the crystallography and NMR system, Nat. Protoc. 2 (2007) 2728–2733.
[33] C.D. Schwieters, J.J. Kuszewski, G.M. Clore, Using Xplor–NIH for NMR molecular structure determination, Prog. Nucl. Magn. Reson. Spectrosc. 48 (2006) 47–62.
[34] B.R. Brooks, R.E. Bruccoleri, B.D. Olafson, D.J. States, S. Swaminathan, M. Karplus, CHARMM: a program for macromolecular energy, minimization, and dynamics calculations, J. Comp. Chem. 4 (1983) 187–217.
[35] S.J. Weiner, P.A. Kollman, D.A. Case, U.C. Singh, C. Ghio, G. Alagona, S. Profeta, P. Weiner, A new force field for molecular mechanical simulation of nucleic acids and proteins, J. Am. Chem. Soc. 106 (1984) 765–784.
[36] A.A.S.T. Ribeiro, B.A.C. Horta, R. Alencatro, MKTOP: a program for automatic construction of molecular topologies, J. Braz. Chem. Soc. 19 (2008) 1433–1435.
[37] R.C. Walker, M.F. Crowley, D.A. Case, The implementation of a fast and accurate QM/MM potential method in amber, J. Comp. Phys. 29 (2008) 1019–1031.
[38] W. Humphrey, A. Dalke, K. Schulten, VMD: visual molecular dynamics, J. Mol. Graph. 14 (1996) 33–38.
[39] N. Guex, M.C. Peitsch, SWISS-MODEL and the Swiss-PdbViewer: an environment for comparative protein modeling, Electrophoresis 18 (1997) 2714–2723.
[40] P.M. Edwards, Origin 7.0: scientific graphing and data analysis software, J. Chem. Inf. Comput. Sci. 42 (2002) 1270–1271.
[41] R. Koradi, M. Billeter, K. Wüthrich, MOLMOL: a program for display and analysis of macromolecular structures, J. Mol. Graph. 14 (1996) 51–55.
[42] D. Warren, The PyMOL Molecular Graphics System, DeLano Scientific, San Carlos, CA, 2002.
[43] M. Kontoyanni, L.M. McClellan, G.S. Sokol, Evaluation of docking performance: comparative data on docking algorithms, J. Med. Chem. 47 (2004) 558–565.
[44] A.R. Leach, B.K. Shoichet, C.E. Peishoff, Prediction of protein–ligand interactions. Docking and scoring: successes and gaps, J. Med. Chem. 49 (2006) 5851–5855.
[45] G.L. Warren, C.W. Andrews, A.M. Capelli, B. Clarke, J. LaLonde, M.H. Lambert, M.S. Head, A critical assessment of docking programs and scoring functions, J. Med. Chem. 49 (2006) 5912–5931.